ChemPubSoc Europe

DOI: 10.1002/cssc.201501506

CHEMSUSCHEM Communications

Hydrogenolysis of Glycerol to 1,3-propanediol under Low Hydrogen Pressure over WO_x-Supported Single/Pseudo-Single Atom Pt Catalyst

Jia Wang[+],[a, b] Xiaochen Zhao[+],[a] Nian Lei,[a, b] Lin Li,[a] Leilei Zhang,[a] Shutao Xu,[c] Shu Miao,[a] Xiaoli Pan,[a] Aiqin Wang,*[a] and Tao Zhang*[a]

Single/pseudo-single atom Pt catalyst was prepared on mesoporous WO_x. The large surface area and abundant oxygen vacancies of WO_x improve the Pt dispersion and stabilize the Pt isolation. This newly prepared catalyst exhibited outstanding hydrogenolysis activity under 1 MPa H_2 pressure with a very high space–time yield towards 1,3-propanediol (3.78 g g_{Pt}^{-1} h^{-1}) in Pt–W catalysts. The highly isolated Pt structure is thought to contribute to the excellent H_2 dissociation capacity over Pt/WO_x. The high selectivity towards 1,3-propanediol is attributed to the heterolytic dissociation of H_2 at the interface of Pt and WO_x (providing specific Brønsted acid sites and the concerted dehydration–hydrogenation reaction) and the bond formation between glycerol and WO_x, which favors/stabilizes the formation of a secondary carbocation intermediate as well as triggers the redox cycle of the W species ($W^{6+} \rightleftarrows W^{5+}$).

Glycerol, a byproduct of the biodiesel and soap synthesis, is available in surplus amounts and requires efficient valorization to high value-added chemicals.[1] Owing to its high oxygen content (C/O = 1), selective hydrogenolysis, whereby C–O bonds are cleaved or undergo lysis by hydrogen, is considered an atom-economical and cost-competitive process.[2] Among the products, 1,3-propanediol (1,3-PD) is the most desirable one due to its wide application as monomer in the polyester industry [polytrimethylene terephthalate (PTT)].[3] However, this reaction is rather challenging as the formation of 1,2-propanediol (1,2-PD) is thermodynamically favored in comparison to 1,3-PD.[1a] In aqueous-phase glycerol hydrogenolysis, Pt-W[4] and Ir-Re[5] catalysts appear to be so far the only effective catalysts with high selectivity to 1,3-PD instead of 1,2-PD.

Generally, H_2 homolytically dissociates to two hydrogen atoms on noble metal sites, which subsequently hydrogenate the dehydrated intermediate formed during hydrogenolysis to target products. Owing to the oxophilic nature of tungsten oxide, the LUMOs of tungsten can capture electrons from H, which results in reduced tungsten and $H^{\delta+}$ and gives rise to Brønsted acidity.[6] This redox cycle[2b,7] is the source of the unique characteristics of tungsten oxide in hydrogen-related reactions. Accordingly, H_2 is expected to heterolytically dissociate to $H^{\delta+}$ (over W) and $H^{\delta-}$ (over Pt) at the interface of Pt and WO_x, respectively, which in turn may be the cause for both dehydration and hydrogenation occurring simultaneously during the reaction. It should be noted that during dehydration, the secondary carbocation is more stable than the primary one; thus, fast stabilization of the secondary carbocation with $H^{\delta-}$ is the key step to achieve a high selectivity to 1,3-PD. Therefore, maximizing the interface between Pt and WO_x may induce optimized heterolytic dissociation of H_2 and lead to a high 1,3-PD selectivity under low H_2 pressure. In other words, the hydrogenolysis performance can be optimized using a good, rational use of H_2, which in turn strongly depends on the chemistry of catalysts and their capacity for H_2 dissociation.

In co-supported Pt–W catalysts, the dispersion of Pt and W species (key for high 1,3-PD selectivity)[4c,e,8] and the acidity of the catalysts (key for high activity) strongly depend on the selected support, which in turn interferes with the elucidation of the true active center and reaction mechanism. For this reason, we employed tungsten oxide alone as the support to rule out subordinate/interferential factors from additional supports; thus, the direct interaction between Pt and W species can be detected, allowing mechanistic insights into structure–activity relationships. Mesoporous WO_x,[9] rich in oxygen vacancies and hydroxyl functionalities, was employed as the support instead of well-crystallized WO_3 because 1) high surface areas may improve Pt dispersion and 2) abundant oxygen vacancies may strengthen the interaction between WO_x and Pt, thereby stabilizing Pt isolation.[10] Herein, we developed a WO_x-supported single/pseudo-single atom Pt catalyst, which exhibited exceptionally high hydrogenolysis activity under low H_2 pressure (1 MPa, other reported catalysts demand a H_2 pressure $>$4 MPa), and the best space–time yield towards 1,3-PD (3.78 g g_{Pt}^{-1} h^{-1}) among all reported results for Pt–W catalysts. Because lower H_2 pressure is desirable in view of reducing the

[a] J. Wang,[+] Dr. X. Zhao,[+] N. Lei, Dr. L. Li, Dr. L. Zhang, Dr. S. Miao, X. Pan, Prof. Dr. A. Wang, Prof. Dr. T. Zhang
State Key Laboratory of Catalysis
Dalian Institute of Chemical Physics
Chinese Academy of Sciences
Dalian 116023 (PR China)
E-mail: aqwang@dicp.ac.cn
taozhang@dicp.ac.cn

[b] J. Wang,[+] N. Lei
University of Chinese Academy of Science
Beijing 100049 (PR China)

[c] Dr. S. Xu
National Engineering Laboratory for Methanol to Olefins
Dalian National Laboratory for Clean Energy
Dalian Institute of Chemical Physics
Chinese Academy of Sciences
Dalian 116023 (PR China)

[+] These authors contributed equally to this work.

Supporting Information for this article can be found under http://dx.doi.org/10.1002/cssc.201501506.

related capital cost in industrial operation, this new Pt/WO_x catalyst, as well as the preparation strategy, is of great significance in H-related reactions.

The textual structures of Pt/WO_x, WO_x, their reference catalyst Pt/WO_3, and the support WO_3 were analyzed using N_2 adsorption–desorption isotherms (Figure S1 in the Supporting Information). The type-IV isotherms with H4 hysteresis indicated that slit mesopores were formed in WO_x and basically maintained in Pt/WO_x. These mesopores were formed by stacks of needle-shaped tungsten suboxide crystals (Figure 1 b), which endowed a larger surface area to WO_x (126 $m^2 g^{-1}$) and the resulting Pt/WO_x catalyst (82 $m^2 g^{-1}$). According to XRD results (Figure S2), the obtained tungsten suboxide was assigned to $WO_{2.8}$ (PDF 00-041-0745) whereas Pt/WO_x and Pt/WO_3 shared a similar crystal structure corresponding to $WO_{2.92}$ (PDF 00-030-1387). Unlike Pt/WO_3, Pt signals could not be detected in the XRD patterns of Pt/WO_x, indicating that smaller Pt particles were formed over WO_x, which is consistent with the TEM results (Figure 1 c and d). To further identify the dispersion and particle size of Pt, high angle annular dark field (HAADF)–STEM was performed; an average particle size of 2.3 nm was estimated for Pt in Pt/WO_3 (Figure 1 e). Surprisingly, although a loading of 2.59 wt% homogeneously dispersed Pt was detected in the mapping area (Figure 1 g), no clear subnano clusters, or even bright single atoms, of Pt were observed in Pt/WO_x (Figure 1 f and Figure S3), suggesting that the Pt species were dispersed at a single or/and pseudo-single atom scale (less than ten atoms Pt-cluster). However, due to the close atomic numbers of Pt and W (only 4 apart), their contrast in HAADF–STEM was too low to obtain an exact number of atom numbers for Pt. In good agreement with H_2 chemisorption results, a microcalorimetric study for H_2 adsorption (Figure 2 a) revealed that over Pt/WO_x the initial H_2 differential heat (108 kJ mol^{-1}) is higher than over Pt/WO_3 (92 kJ mol^{-1}) whereas the H_2 uptake over Pt/WO_x is also larger than that over Pt/WO_3.[11] This further convinced us that Pt is highly dispersed on WO_x. As most studies suggested that H_2 was dissociated on Pt–Pt sites, we further investigated why an enhanced H_2 dissociation capacity is obtained on this single/pseudo-single atom Pt catalyst. The as-prepared catalyst without reduction was first characterized as reference using in situ X-ray photoelectron spectroscopy (XPS; Figure 2 b); following an in situ reduction at 573 K for 1 h, the Pt/WO_x catalyst was again analyzed to monitor the effect of H_2 during the reduction. Clearly, two new W species were generated after H_2 reduction; W3 is assigned to the oxidation of W1 whereas W2 is assigned to the reduction of W1. We attribute the appearance of these two new W species to the heterolytical H_2 dissociation over tungsten oxide whereas dissociated $H^{\delta+}$ and $H^{\delta-}$ gave rise to the oxidation and the reduction reactions, respectively.

In addition, we also attempted to use in situ CO-adsorption FTIR spectroscopy to distinguish between linear and bridge bond formation of CO adsorption[10c] to identify single/pseudo-single atom Pt. However, for Pt/WO_x, the adsorption of CO was too weak to withstand evacuation and only gas-phase CO was detected. This indirectly confirmed that Pt was highly dispersed on WO_x, but it would still be adventurous to clarify whether the dispersion of Pt is on a single-atom scale. Therefore, we called the catalyst WO_x-supported single/pseudo-single atom Pt catalyst.

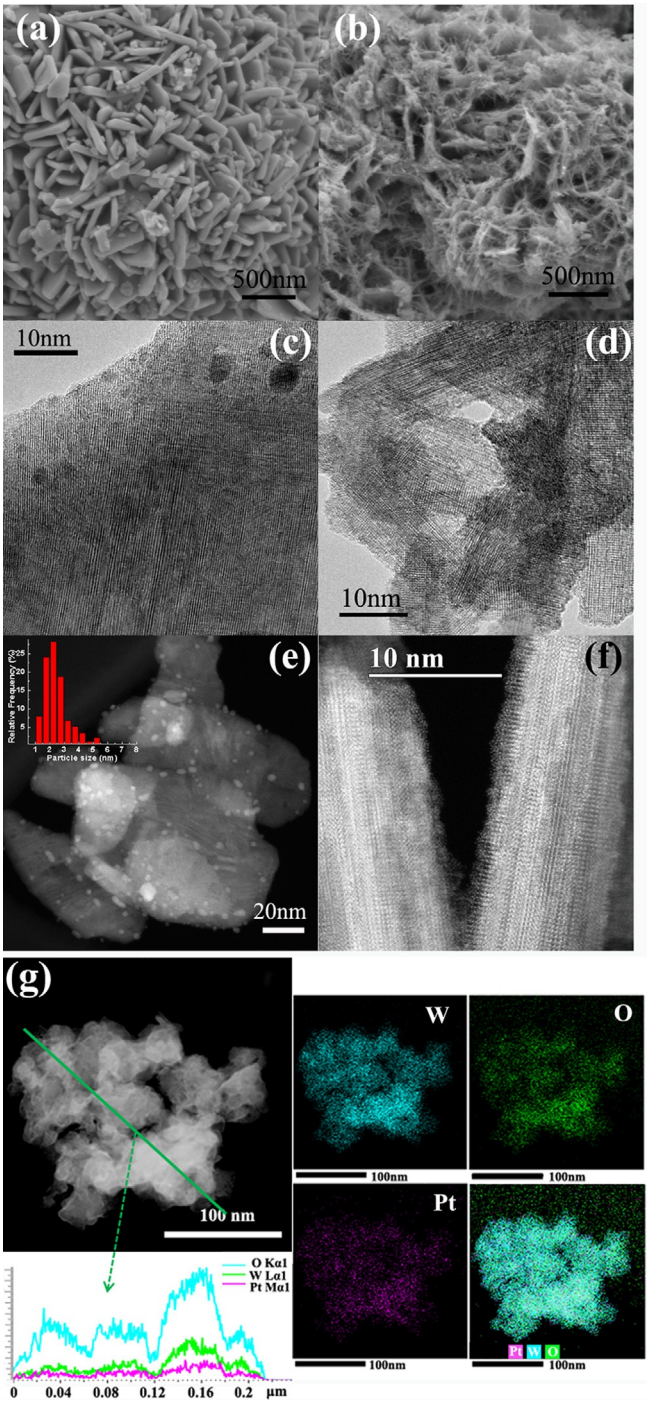

Figure 1. SEM images for (a) WO_3 and (b) WO_x; TEM images for (c) Pt/WO_3 and (d) Pt/WO_x; HAADF–STEM images for (e) Pt/WO_3 and (f) Pt/WO_x; (g) EDS-mapping images of W, O, Pt for Pt/WO_x.

This high dispersion of Pt suggests a strong interaction between Pt and WO_x, which could be attributed to the presence of oxygen vacancies in WO_x (Figure S2 XRD and Figure S4 UV/Vis). As dissociated Pt^{4+} species come in contact with W^{5+}, they tended to remain at the vacancies and were reduced to

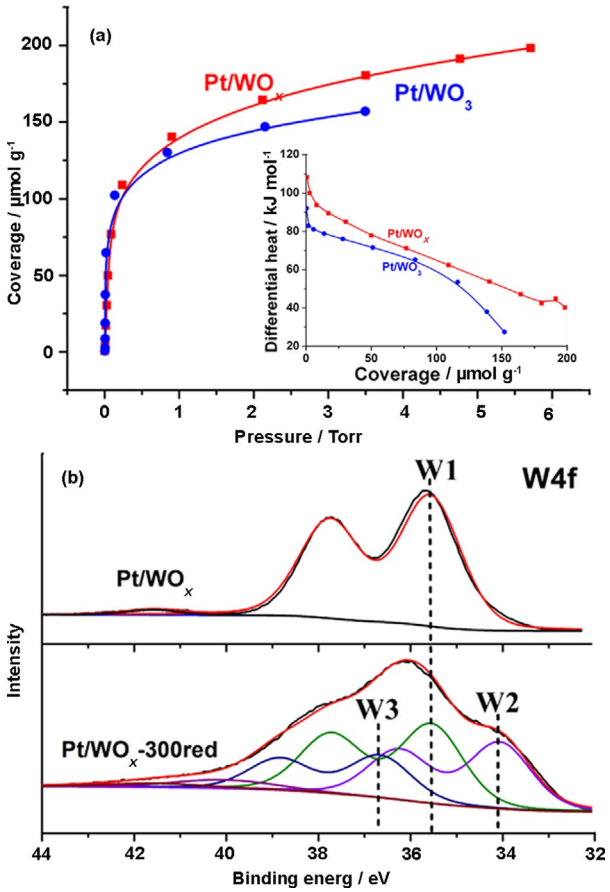

Figure 2. (a) Isotherms and differential heat of H_2 adsorption on Pt/WO_x and Pt/WO_3; (b) in situ XPS results for Pt/WO_x and reduced Pt/WO_x.

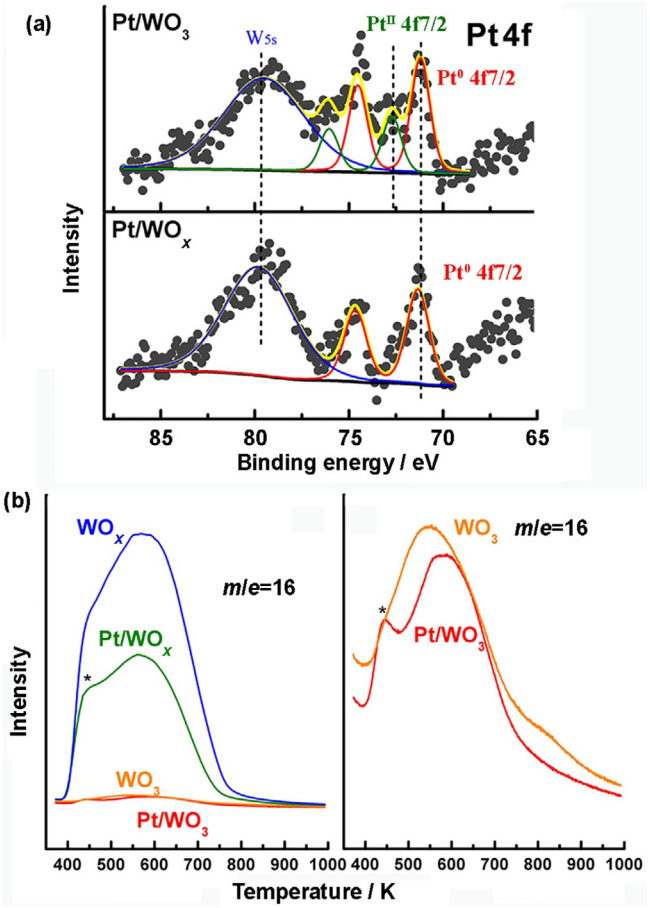

Figure 3. (a) XPS patterns of Pt 4f for Pt/WO_x and Pt/WO_3. (b) NH_3-TPD (*m/e* = 16) curves of Pt/WO_x, Pt/WO_3, WO_x, and WO_3. Enlarged signals of WO_3 and Pt/WO_3 are on the right.

less positive Pt species whereas W^{5+} was oxidized to W^{6+} (evidenced by the color change of WO_x after Pt impregnation, Figure S5).[9] This in situ redox reaction occurred at the interface simultaneously as the impregnation began, and in turn, significantly influenced the subsequent reduction behavior.[9] According to H_2 temperature-programmed reduction (TPR) results (Figure S6), the reduction temperature of Pt in Pt/WO_x (355 K) is much higher than that in Pt/WO_3 (276 K). Generally, a small particle size will facilitate the kinetics of reduction and allow a lower reduction temperature unless the strong metal support interaction (SMSI) plays an overwhelming role in suppressing the Pt reduction. Combined with the electron microscopy images in Figure 1, we attribute the higher Pt reduction temperature in Pt/WO_x to the SMSI effect. For Pt/WO_3, H_2 consumed for the sharp peak centered at 275 K is calculated to stoichiometrically reduce PtO_2 to Pt; for Pt/WO_x, the first peak centered at 355 K takes up almost twice the amount of H_2 as Pt/WO_3, implying that besides Pt some adjacent W species were reduced simultaneously.

The first peak is directly followed by a distinct reduction occurring at roughly 367 K, attributed to the reduction of less strongly interacting W species. Unlike previously reported, single-atom/subnano cluster catalysts bearing very small amounts of Pt group metals,[10] the Pt loading on WO_x was as high as 2 wt% and could thus be analyzed by XPS (Figure 3a). In the patterns of Pt 4f, only one species (Pt^0) could be detected in Pt/WO_x, which in contrast to Pt/WO_3 for which both Pt^0 and Pt^{II} species were found. We attributed the homogeneous presence of Pt^0 to the SMSI that prevented the oxidation of metallic Pt into Pt^{II} even after exposure to air. The surface acid sites present on 2 wt% Pt/WO_x and Pt/WO_3 were characterized by NH_3 temperature-programmed desorption (TPD; Figure 3b). After loading of Pt, clear weak-acid peaks appeared at around 430 K over both WO_x and WO_3, which can be attributed to the hydroxyl groups on tungsten atoms associated with Pt.[12] Estimated from the NH_3 adsorption amount, the acid-site densities of Pt/WO_x increased from 6.38 (WO_x) to 7.95 μmol m^{-2} after loading with Pt and were slightly larger than that of Pt/WO_3 (Table 1). All acid sites over Pt/WO_x and Pt/WO_3 were assigned to weak–middle strength acids, and most of them were confirmed as Brønsted acids by ^{31}P NMR spectroscopy. To evaluate the performance for glycerol hydrogenolysis over the as-prepared Pt/WO_x catalysts, first conventional reaction conditions[13] (413 K, 5.5 MPa H_2) were employed over Pt/WO_x and its referencePt/WO_3. Although the conversion of glycerol and the ratio of 1,3-PD/1,2-PD over Pt/WO_x is improved compared to that over Pt/WO_3 (Table 2, entries 3 and 4), the absolute conversion of glycerol and the yield of 1,3-PD is relatively low compared to the best results reported so far.

Table 1. Textural parameters, acid properties, and H_2 uptakes of Pt/WO_x, Pt/WO_3, and their supports.

Sample	S_{BET}[a] [$m^2 g^{-1}$]	D_{pore}[b] [nm]	Acid density[c] [$\mu mol\, m^{-2}$]	H_2 uptake [$mmol\, g^{-1}$]
Pt/WO_x	82	6.5	7.95	0.137
WO_x	126	3.4	6.38	–
Pt/WO_3	16	20.4	6.06	0.096
WO_3	17	18.5	6.88	–

[a] Brunauer–Emmett–Teller surface area. [b] The average pore diameters. [c] Acid densities were calculated according to the amount of adsorbed NH_3.

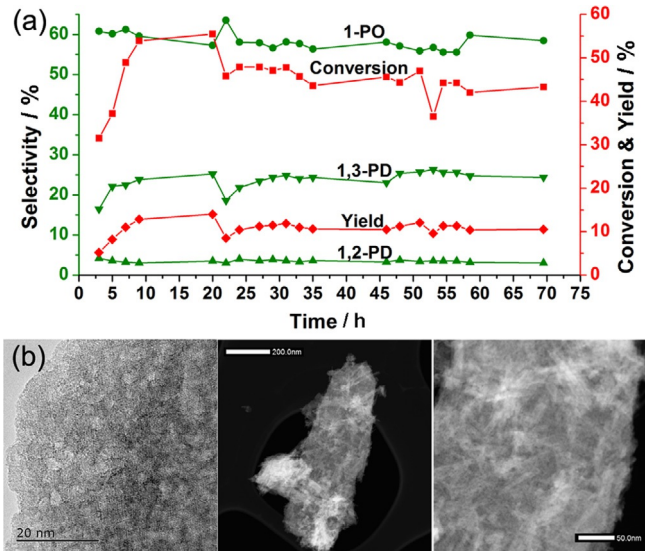

Figure 4. (a) Stability test of Pt/WO_x was conducted in fixed-bed reactor at 413 K, 1.0 MPa, gas hourly space velocity GHSV = 1000 h^{-1}, liquid hourly space velocity LHSV = 1 h^{-1}, with 5 wt% glycerol. (b) TEM (left) and HAADF-STEM images of the used Pt/WO_x catalyst (middle and right; scale bars correspond to 200 and 50 nm).

However, optimization of reaction conditions revealed an exciting catalytic behavior over Pt/WO_x: the conversion of glycerol greatly increased, without compromising the 1,3-PD selectivity, as a negative function of H_2 pressure [up to 1.0 MPa; Tables 2 entry 6 and S1; the high ratio of 1,3-PD/1,2-PD was attributed to the likely secondary reaction of 1,2-PD to 1-propanol (1-PO) (Table S1)]. This behavior was not observed on Pt/WO_3.Therefore, compared with Pt/WO_3, the 1,3-PD/1,2-PD ratio increased from 3.4 to 13.1 over Pt/WO_x when reducing the H_2 pressure from 5.5 to 1.0 MPa (Table 2, entries 5 and 6). The calculated space–time yield of 1,3-PD for Pt/WO_x is approximately 3.78 $g\, g_{Pt}^{-1}\, h^{-1}$, to the best of our knowledge the highest space–time yield reported on Pt–W catalysts to date (Tables 2, entry 10 and S2). Moreover, this value was obtained under a H_2 pressure of 1 MPa, much milder than other reported reaction conditions, which would drastically reduce the capital cost in practical industry. To rule out the influence of surface areas and consequently variance of Pt dispersion and acid-site amount, a control experiment was conducted employing 8 times of WO_3 as support but keeping the amount of Pt loaded constant (Figure S8 and Table 2, entry 8). The results showed that the surface area and the amount of acid sites play very limited roles in reactivity improvement; however, the Pt dispersion and its associated acid sites are crucial in this reaction. Taking advantage of the mild reaction conditions, Pt/WO_x exhibited a promising stability in 75 h run without noticeable agglomeration of Pt (Figure 4).

Generally, a higher hydrogen pressure is favorable for hydrogenolysis. In this work, however, the best performance was obtained under circa 1 MPa H_2; increasing H_2 pressure afterwards resulted in a decreased glycerol conversion. According to the H_2 chemisorption results (Table 1), we attribute this uncommon shift to lower pressure to the superior dissociating H_2 capacity over the WO_x-supported single/pseudo-single atom Pt catalyst, which facilitated the hydrogenolysis of glycerol under low H_2 pressure and, conversely, "poisoned" the catalysts under high H_2 pressure. Comparison of the used catalysts under 1 and 5.5 MPa showed that higher H_2 pressure may further reduce W^{5+} to W^{4+} (Figure 5), which limits the catalytic redox cycle of

Table 2. Hydrogenolysis of glycerol over tungsten oxide supported Pt catalysts.[a]

Entry	Catalyst	T [K]	P_{H_2} [MPa]	Conv.[b] [%]	Selectivity [%] 2-PO	1-PO	1,2-PD	1,3-PD	others[c]	1,3-PD/1,2-PD	$Yield_{1,3\text{-PD}}$ [%]
1	WO_3	413	5.5	–							
2	WO_x	413	5.5	–							
3	2%Pt/WO_3	413	5.5	3.2	4.9	31.2	9.9	43.7	10.3	4.4	1.4
4	2%Pt/WO_x	413	5.5	14.2	5.2	47.4	1.1	33.0	13.3	29.6	4.7
5	2%Pt/WO_3	413	1.0	2.2	3.9	36.2	5.9	45.7	8.3	7.7	1.0
6	2%Pt/WO_x	413	1.0	37.4	5.1	50.3	2.3	35.1	7.3	15.3	13.1
7	2%Pt/WO_x	433	1.0	49.5	4.1	52.3	6.5	28.1	9.0	4.3	13.9
8[d]	2%Pt/WO_3	413	1.0	6.0	7.2	52.8	4.6	27.8	7.6	6.0	1.6
9[e]	2%Pt/WO_x	413	1.0	6.6	0.0	40.9	10.3	43.1	5.7	4.2	2.9
10[e]	2%Pt/WO_x	433	1.0	16.1	4.3	45.8	10.6	34.0	5.3	3.2	5.5
11[f]	2%Pt/WO_x	413	1.0	59.8	5.8	48.2	3.1	36.3	6.6	11.7	21.7

[a] The conversion deviation is ±4.5%, the 1,3-PD selectivity deviation is ±6.3%. [b] Typical reaction conditions: 12 g 5 wt% glycerol aqueous solution in 75 mL autoclave with Teflon lining, 0.3 g of catalyst, stirring at 800 rpm, 413 K, 12 h. [c] Others include propylene, ethylene glycol, ethanol, methanol, methane, and ethane. [d] 2.4 g 0.25%Pt/WO_3 catalysts were employed under the reaction conditions of 413 K, 12 h, and H_2 pressure 1.0 MPa. [e] 12 g 50 wt% glycerol aqueous solution was used as the substrate. [f] the amount of catalysts is doubled to 0.6 g.

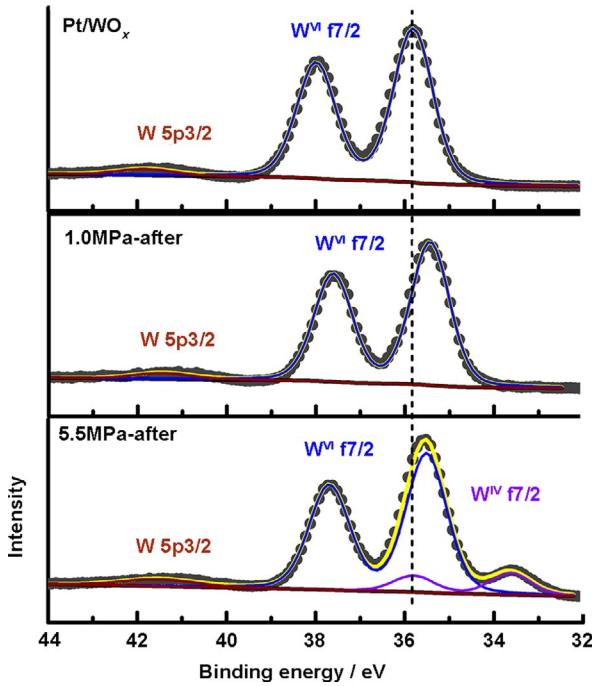

Figure 5. W 4f XPS spectra of fresh and used Pt/WO_x under 1 and 5.5 MPa H_2, respectively.

$W^{6+} \rightleftarrows W^{5+}$ and in turn decreases the activity under high H_2 pressure.

To further understand the hydrogenolysis process, a series of in situ characterizations were conducted on Pt/WO_x as a function of reaction time to monitor the variance of W state (Figure 6). In Raman spectra, three strong bands at 706, 785, and 959 cm^{-1} were detected in Pt/WO_x (Figure 6a). The former two were assigned as ν(O–W–O) modes of the bridging oxygen atoms in the WO_6 octahedra, whereas the latter one was assigned to the stretching mode of the terminal W=O bond on the surface, which can extract protons in many surface reactions.[14] The terminal-W=O band (959 cm^{-1}) decreased dramatically after coming in contact with glycerol whereas the 785 cm^{-1} band was shifted to 796 cm^{-1} and the 706 cm^{-1} band, sensitive to cation intercalation,[6,15] decreased slightly. This change implies that the W=O bond was cleaved after the adsorption of glycerol whereas WO_x was reduced by the inserted proton. In situ X-ray absorption near edge structure (XANES) spectra further evidenced this implication, in which the general valence of W was shown to gradually decrease from the beginning of the reaction (Figure 6b).

Inspired by the photochromism of tungsten oxide[16] and taken all current characterization and performance results together, we, therefore, proposed a reaction scheme as following (Scheme 1):

First, the unshared-pair electrons of oxygen atoms in glycerol were trapped by the unoccupied d orbital of W^{6+}, forming an ether-like bond with a W atom. The strong interaction with the W atom, in turn, weakened the bond between the O and H atoms and facilitated the oxidation of a H atom. The proton was then extracted by the terminal O atom of W=O to form

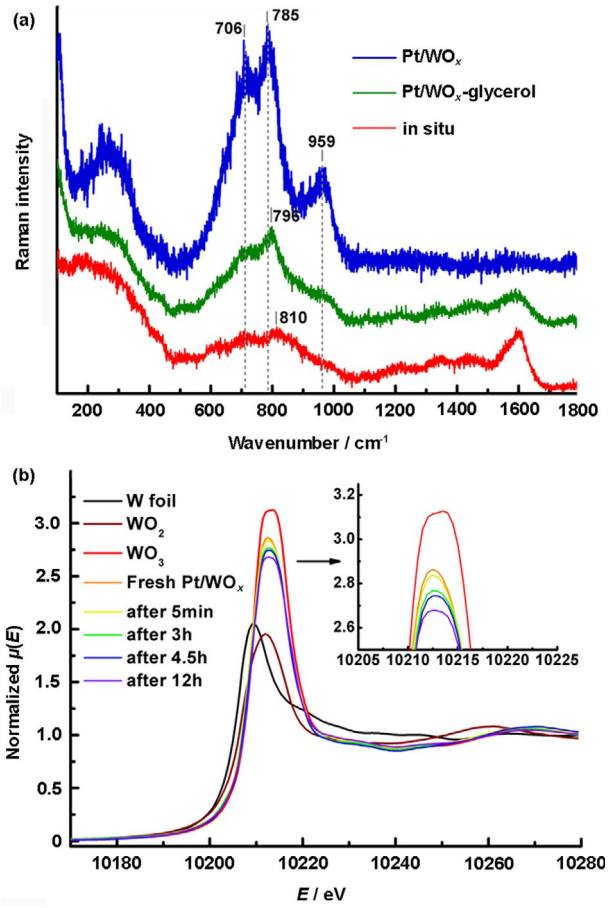

Figure 6. (a) Raman spectra of Pt/WO_x, Pt/WO_x impregnating in glycerol, and in situ Raman spectra of Pt/WO_x in glycerol at 413 K under H_2 atmosphere after 3 h. (b) in situ XANES spectra at W L_3 edge; the sample after 12 h (purple) corresponds to the used catalysts.

W–OH (Figure 6a) whereas W^{6+} was partially reduced (Figure 6b), which is consistent with our previous study employing Ti–W composite oxide as the support.[13] After the "adsorption" of glycerol, Brønsted acid sites were consumed, catalyzing the dehydration of glycerol (Figure S7). In contrast to the usually formed H bond between glycerol and metal oxide supports, the strengthened bonding with WO_x favored/stabilized the formation of the secondary carbocation from glycerol. Moreover, owing to the oxophilic nature of W, H_2 is assumed to be heterolytically dissociated on the interface between Pt and WO_x, exhibiting both acid sites ($H^{\delta+}$) and hydrogenation sites ($H^{\delta-}$). This characteristic speeds up the hydrogenation of 3-hydroxypropanal before it transforms to the thermodynamically favored acetol and gives rise to a high selectivity to 1,3-PD. In this work, the interface between Pt and WO_x was maximized by the design of a single/pseudo-single atom Pt catalyst, and thus high H_2 pressure was unnecessary to increase the hydrogenation rate.

In summary, a new WO_x-supported single/pseudo-single atom Pt catalyst was designed by employing large surface area, mesoporous tungsten suboxide as the support. In the selective hydrogenolysis of glycerol, a productivity of 3.78 g g_{Pt}^{-1} h^{-1} was achieved for 1,3-PD over Pt/WO_x, to the

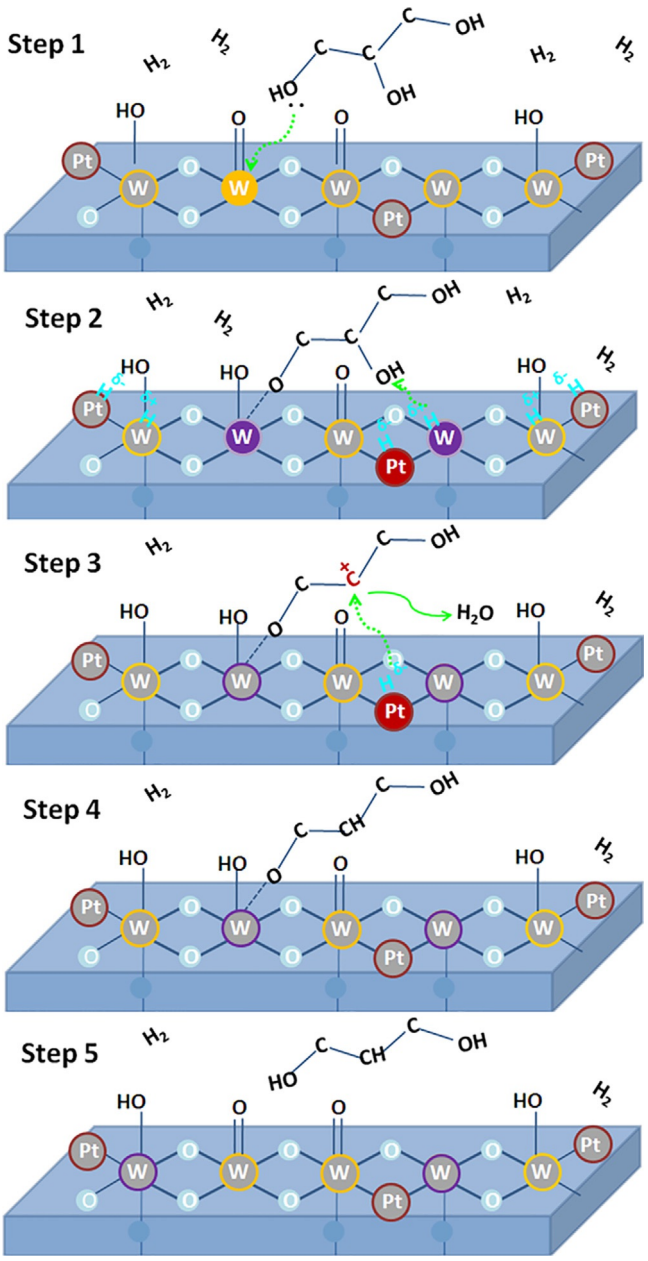

Scheme 1. Proposed reaction scheme for hydrogenolysis of glycerol to 1,3-PD over Pt/WO_x.

best of our knowledge, the highest space–time yield among all reported results over Pt–W catalysts. Moreover, this performance was obtained under mild conditions (433 K, 1 MPa H_2) using a relatively high glycerol concentration (50%), which means a great cost reduction in industrial operation. The trends in characterizations and performances allowed mechanistic insight into the structure–activity relationship and further enabled the optimization of reaction conditions and catalyst preparation. In the current study, precise identification of Pt atoms are still challenging owing to the close atomic number of W and Pt; therefore, efficient characterization and theoretical calculations to clarify/support the isolation of Pt over WO_x are highly desired. In addition, due to the unique photochromic characteristics of tungsten oxide, the application of this new Pt/WO_x catalyst can be further extended to photocatalysis and photo-electrocatalysis.

Experimental Section

WO_x was prepared using a modified procedure according to Xi et al.[9] In detail, WCl_6 (3 g) (Aladdin) was added to ethanol (100 mL) while stirring mildly for 20 min and then transferred to a Teflon-lined autoclave and heated in an oven at 433 K for 36 h. After cooling to room temperature, dark blue products were recovered, which were washed with ethanol and water. WO_x was obtained by drying the as-prepared samples at 323 K for 6 h in vacuum. Pt/WO_x was prepared by impregnating WO_x with H_2PtCl_6 solution (6.7 wt%; Tianjin Fengchuan Chemical Reagent Technologies Co., Ltd., Pt >37.0%) overnight before drying at 323 K for 6 h in vacuum and then reducing in flowing H_2 at 573 K for 1 h; the catalyst was then passivated using 1% O_2/N_2 for 4 h at room temperature. Pt/WO_3 was prepared by impregnating WO_3 with H_2PtCl_6 (same conditions as above) overnight and drying at 373 K overnight, which was followed by calcination at 673 K for 1 h. The catalyst was then reduced in flowing H_2 at 573 K for 1 h, and passivated with 1% O_2/N_2 for 4 h at room temperature.

Catalytic activities were carried on in a 75 mL of autoclave with Teflon lining. Typically, catalyst (0.3 g) and glycerol aqueous solution (12 g; 5 wt%; Tianjin Kermel Chemical Reagent Co., Ltd. >99.0%) were put into the autoclave and flushed with H_2 several times. The reaction was conducted at 413 K and 1 MPa H_2 for 12 h. The gas and the liquid products were collected and analyzed separately. The conversion (conv.) of glycerol and the selectivity (sel.) of each liquid product were calculated using Equations (1) and (2), respectively:

$$\text{Conv.}\ [\%] = (\text{mol}_{\text{glycerol consumed}})/(\text{mol}_{\text{glycerol initially added}}) \times 100 \quad (1)$$

$$\text{Sel.}\ [\%] = (\text{mol}_{\text{carbon in specific product}})/(\text{mol}_{\text{carbon in consumed glycerol}}) \times 100. \quad (2)$$

Acknowledgements

The authors appreciate financial support by the National Natural Science Foundation of China (21176235, 21373206, and 21303187). The authors greatly thank Leifeng Gong and Hua Wang for product analysis, Xiong Su for solid-acid-analysis discussions, Botao Qiao for single-atom-catalysis discussions, and Guanfeng Liang, Longjie Liu, Chaojun Yang, and Yao Wang for fruitful discussions.

Keywords: 1,3-propanediol · glycerol · hydrogenolysis · supported catalysts · tungsten oxide

[1] a) J. ten Dam, U. Hanefeld, *ChemSusChem* **2011**, *4*, 1017–1034; b) Y. Nakagawa, M. Tamura, K. Tomishige, *J. Mater. Chem. A* **2014**, *2*, 6688; c) C.-H. Zhou, J. N. Beltramini, Y.-X. Fan, G. Q. Lu, *Chem. Soc. Rev.* **2008**, *37*, 527–549.

[2] a) A. M. Ruppert, K. Weinberg, R. Palkovits, *Angew. Chem. Int. Ed.* **2012**, *51*, 2564–2601; *Angew. Chem.* **2012**, *124*, 2614–2654; b) N. Ota, M. Tamura, Y. Nakagawa, K. Okumura, K. Tomishige, *Angew. Chem. Int. Ed.* **2015**, *54*, 1897–1900; *Angew. Chem.* **2015**, *127*, 1917–1920.

[3] A. Martin, M. Richter, *Eur. J. Lipid Sci. Technol.* **2011**, *113*, 100–117.

[4] a) S. Zhu, X. Gao, Y. Zhu, Y. Li, *J. Mol. Catal. A* **2015**, *398*, 391 – 398; b) S. García-Fernández, I. Gandarias, J. Requies, M. B. Güemez, S. Bennici, A. Auroux, P. L. Arias, *J. Catal.* **2015**, *323*, 65 – 75; c) R. Arundhathi, T. Mizugaki, T. Mitsudome, K. Jitsukawa, K. Kaneda, *ChemSusChem* **2013**, *6*, 1345 – 1347; d) J. ten Dam, K. Djanashvili, F. Kapteijn, U. Hanefeld, *ChemCatChem* **2013**, *5*, 497 – 505; e) L.-Z. Qin, M.-J. Song, C.-L. Chen, *Green Chem.* **2010**, *12*, 1466 – 1472.

[5] a) Y. Nakagawa, Y. Shinmi, S. Koso, K. Tomishige, *J. Catal.* **2010**, *272*, 191 – 194; b) Y. Amada, Y. Shinmi, S. Koso, T. Kubota, Y. Nakagawa, K. Tomishige, *Appl. Catal. B* **2011**, *105*, 117 – 127; c) Y. Nakagawa, X. Ning, Y. Amada, K. Tomishige, *Appl. Catal. A* **2012**, *433 – 434*, 128 – 134; d) J. Guan, X. Chen, G. Peng, X. Wang, Q. Cao, Z. Lan, X. Mu, *Chin. J. Catal.* **2013**, *34*, 1656 – 1666.

[6] D. G. Barton, M. Shtein, R. D. Wilson, S. L. Soled, E. Iglesia, *J. Phys. Chem. B* **1999**, *103*, 630 – 640.

[7] T. Yang, Y. Zhang, C. Li, *J. Alloys Compd.* **2014**, *584*, 546 – 552.

[8] a) T. Kurosaka, H. Maruyama, I. Naribayashi, Y. Sasaki, *Catal. Commun.* **2008**, *9*, 1360 – 1363; b) L. Gong, Y. Lu, Y. Ding, R. Lin, J. Li, W. Dong, T. Wang, W. Chen, *Appl. Catal. A* **2010**, *390*, 119 – 126.

[9] G. Xi, J. Ye, Q. Ma, N. Su, H. Bai, C. Wang, *J. Am. Chem. Soc.* **2012**, *134*, 6508 – 6511.

[10] a) J. Lin, B. Qiao, J. Liu, Y. Huang, A. Wang, L. Li, W. Zhang, L. F. Allard, X. Wang, T. Zhang, *Angew. Chem. Int. Ed.* **2012**, *51*, 2920 – 2924; *Angew. Chem.* **2012**, *124*, 2974 – 2978; b) H. Wei, X. Liu, A. Wang, L. Zhang, B. Qiao, X. Yang, Y. Huang, S. Miao, J. Liu, T. Zhang, *Nat. Commun.* **2014**, *5*, 5634; c) B. Qiao, A. Wang, X. Yang, L. F. Allard, Z. Jiang, Y. Cui, J. Liu, J. Li, T. Zhang, *Nat. Chem.* **2011**, *3*, 634 – 641; d) X.-F. Yang, A. Wang, B. Qiao, J. Li, J. Liu, T. Zhang, *Acc. Chem. Res.* **2013**, *46*, 1740 – 1748.

[11] a) L. Li, X. Wang, X. Zhao, M. Zheng, R. Cheng, L. Zhou, T. Zhang, *Thermochim. Acta* **2005**, *434*, 119 – 124; b) D. Uner, M. Uner, *Thermochim. Acta* **2005**, *434*, 107 – 112.

[12] a) D. Hibbitts, Q. Tan, M. Neurock, *J. Catal.* **2014**, *315*, 48 – 58; b) M. Chia, Y. J. Pagán-Torres, D. Hibbitts, Q. Tan, H. N. Pham, A. K. Datye, M. Neurock, R. J. Davis, J. A. Dumesic, *J. Am. Chem. Soc.* **2011**, *133*, 12675 – 12689.

[13] Y. Zhang, X.-C. Zhao, Y. Wang, L. Zhou, J. Zhang, J. Wang, A. Wang, T. Zhang, *J. Mater. Chem. A* **2013**, *1*, 3724 – 3732.

[14] C. Santato, M. Odziemkowski, M. Ulmann, J. Augustynski, *J. Am. Chem. Soc.* **2001**, *123*, 10639 – 10649.

[15] a) S. Balaji, A.-S. Albert, Y. Djaoued, R. Brüning, *J. Raman Spectrosc.* **2009**, *40*, 92 – 100; b) S. Balaji, Y. Djaoued, A.-S. Albert, R. Bruning, N. Beaudoin, J. Robichaud, *J. Mater. Chem.* **2011**, *21*, 3940 – 3948.

[16] a) U. Tritthart, W. Gey, A. Gavrilyuk, *Electrochim. Acta* **1999**, *44*, 3039 – 3049; b) N. Tahmasebi Garavand, M. Ranjbar, S. M. Mahdavi, A. Irajizad, *Appl. Surf. Sci.* **2012**, *258*, 10089 – 10094.

Received: November 8, 2015
Revised: December 19, 2015
Published online on February 23, 2016